cent of the TOC in the solutions. Edax spectra for these amorphous organic particles show minor amounts of Al, Fe, P, S, and Si. The presence of Al and Fe in the Edax spectra illustrates the active role of the organic components in transferring these metals through the soil.

To determine the effect of air-drying on the shape of the organic particles, freeze-dried filters from O2 and A2 were also examined. The freeze-dried, filtered material from O2 was much different from its air-dried equivalent. The freeze-dried organic material consists of filaments 5 to 12 μm long emanating from oblong bodies as compared to the distinct, smooth air-dried particles (Fig. 1). Both air- and freeze-dried organic particles from A2 appear to have the same shape and size.

Figure 2 shows particular material collected below IIB2hir. The difference between Figs. 1 and 2 is striking. Solutions percolating through O2 and A2 are mainly charged with mobile organic particles. In passing through IIB2hir, these organic bodies are arrested, and the solutions become charged almost exclusively with mineral particles. These mineral particles range in size from about 2.0 to 22 μm, with 8-μm particles predominating. Edax spectra for a number of the inorganic particles show a prevalence of silicate minerals containing Si, Al, and minor quantities of Fe, Ca, and K. The high Fe content of other particles indicates the presence of pyroxene or amphibole minerals. X-ray analysis of the Nuclepore filter retaining the inorganic particles reveals diffraction lines for chlorite, feldspars, and quartz. Chlorite, however, is the dominant mineral, and it is thought to be of pedogenic origin, the same as detected in IIIB31 (*14*). Solutions collected within the IVB32 have the same silicate load and the same elemental composition as those below IIB2hir. Clay minerals for the horizon below IIB2hir show the predominance of pedogenic chlorite and vermiculite. Figure 2 suggests the illuvial origin of at least a portion of these phyllosilicates.

This study indicates that the suspended material in the soil solution reflects the same trend as the solution itself. The reduction in the TOC and the 60 to 70 percent reduction of the fulvic acids as the solution passes through IIB2hir are verified by the presence of organic particles in Fig. 1 and their absence in Fig. 2.

This study provides direct evidence for the mechanism of podzolization. It shows that mineral particles, mostly phyllosilicates and feldspars from 2 to 22 μm, are mobilized in IIB2hir and transported at depth. The B2hir horizon of this Podzol is primarily an illuvial horizon for the suspended organics and complexed metals and an eluvial horizon for the silicates. The scanning electron micrograph and Edax proved to be excellent tools for studying suspended particles in the soil solution and for clarifying one of the theories of soil-forming processes.

F. C. UGOLINI
H. DAWSON
J. ZACHARA
College of Forest Resources, University of Washington, Seattle 98195

References and Notes

1. We prefer to call this soil a Podzol rather than the current term Spodosol because, in spite of having the morphology and chemistry of a Spodosol, it fails to meet the strict criteria of soil taxonomy of a Spodosol (Handbook No. 436, U.S. Department of Agriculture, Washington, D.C., 1975). Similar soils are called Ferro-Humic Podzols in the Canadian soil classification system. Because the original field description for the Podzol profile makes use of specific terminology, an abridged and less technical version is given in Table 1.
2. The term "soil solution" traditionally represents the liquid phase in the soil. We use "soil solution" here to mean both solute and suspended components; in actuality, the soil solution is a suspension.
3. D. W. Cole, *Water Resour. Res.* **4**, 1127 (1968).
4. R. M. Hirsh, thesis, University of Washington (1975).
5. M. Rubin and C. Alexander, *Am. J. Sci. Radiocarbon Suppl.* **2**, 129 (1960).
6. J. G. Bockheim and F. C. Ugolini, "Coniferous Forest Biome" (College of Forest Resources, University of Washington Internal Report 47, Seattle, 1972).
7. D. R. Crandell, D. R. Mullineaux, M. Rubin, *Science* **187**, 438 (1975).
8. E. L. Phillips, Miscellaneous Publication 2734 (Cooperative Extension Service, Washington State University, Pullman, 1968).
9. R. Del Moral, *Am. Midl. Nat.* **89**, 26 (1973).
10. J. Turner and M. J. Singer, *J. Appl. Ecol.* **13**, 295 (1976).
11. F. C. Ugolini, R. Minden, H. Dawson, J. Zachara, H. Riekerk, in preparation.
12. D. W. Johnson, thesis, University of Washington (1975).
13. R. F. Christman, thesis, University of Florida (1962).
14. M. Singer and F. C. Ugolini, in preparation.
15. References to trade names of material and equipment used in this study do not constitute endorsement. Supported by NSF grant GB36810X to the Coniferous Forest Biome (Contribution No. 272), Ecosystem Analysis Studies, U.S.-International Biological Program. We thank Mrs. K. Trafton for assistance in the laboratory and Dr. J. A. Kittrick for suggesting that we freeze-dry the filters.

17 March 1977; revised 16 June 1977

Interstitial Nitrate Profiles and Oxidation of Sedimentary Organic Matter in the Eastern Equatorial Atlantic

Abstract. *Pore-water nitrate concentrations in six pelagic eastern equatorial Atlantic cores increase from bottom water values (22 micromolar) to 40 micromolar at a depth of about 5 centimeters, then decrease to undetectable levels at depths as shallow as 40 centimeters. These nitrate concentrations and concentration gradients reflect zones of oxygen reduction, nitrate reduction, and sulfate reduction in the sediments. The estimated benthic flux of nitrate to the ocean from our data is much less than the total global flux of nitrate to deep waters, even though these equatorial sediments underlie a productive upwelling zone. The estimated denitrification rate in our study area suggests that pelagic sediments may be important sites of marine denitrification.*

Inorganic carbon, nitrogen, and phosphorus are fixed into organic matter at the sea surface during photosynthesis. A small portion of the particulate organic matter is delivered to the deep sea and incorporated into marine sediments. The organic matter thus buried is partly oxidized and regenerated within the sediment by oxidants (O_2, NO_3^- plus NO_2^-, and SO_4^{2-}) which are either derived from pore waters, provided by diffusion from the overlying water, or produced by diagenetic reactions within the sediment column (NO_3^- plus NO_2^- only). Metabolites, oxidants, and reductants are all present in pore waters. Concentrations of these products are controlled by C : N : P ratios in the organic matter undergoing diagenesis, by relative rates of diffusion, and by rates of reaction, sedimentation, and bioturbation (*1*).

The purpose of this report is to discuss the fate of nitrate produced by diagenetic reactions in a suite of cores from the Guinea Basin in the eastern equatorial Atlantic, to show that pore-water nitrate profiles can provide much information about the early diagenesis of deep-sea sediments, and to make preliminary assessments of the global significance of the pelagic benthic flux of nitrate and pelagic denitrification.

Before discussing the pore-water data, it is worthwhile to review a simple model of organic diagenesis (*2*–*4*). In doing so we will make the following simplifying assumptions: (i) all the organic matter undergoing oxidation has C : N : P atom ratios of 106 : 16 : 1 (the Redfield ratios); (ii) there are no solid-phase reactions (other than the breakdown of organic matter itself) releasing metabolities to or consuming them from pore waters; (iii) ammonia released by deamination during oxidation of organic matter by dissolved oxygen is immediately con-

Table 1. Gravity core locations.

Identification	Location	Water depth (m)	Length (cm)
G76-5-7GC1	4°59.5′N, 5°09.2′W	55	60
G76-5-10GC1	1°05.1′N, 8°11.6′W	4956	65
G76-5-11TW1*	0°01.8′N, 9°03.9′W	4980	89
G76-5-12GC1, G76-5-12GC2	0°04.1′N, 10°33.8′W	3880	63, 90
G76-5-14GC1	0°00.1′S, 12°19.3′W	4170	63
G76-5-16GC1, G76-5-16GC2	0°02.5′S, 16°07.1′W	3310	48, 63
G76-5-23GC1	1°06.0′N, 8°12.5′W	4901	55
G76-5-27GC1	4°59.1′N, 5°06.0′W	80	64
G76-5-28GC1	4°55.9′N, 5°05.4′W	229	43

*Trigger weight core.

verted to nitrate; and (iv) the initial pore fluids (before any reactions commence) contained the same metabolite concentrations as local bottom water (ΣCO_2, 2185 μM; O_2, 250 μM; NO_3^-, 22 μM; PO_4^{3-}, 1.45 μM; and SO_4^{2-}, 28.81 mM; see Fig. 1, point A).

In oxygenated sediments, the degradation of organic matter can be described by the relation

$$5\ (CH_2O)_{106}(NH_3)_{16}(H_3PO_4) + 690\ O_2 \rightarrow 530\ CO_2 + 80\ HNO_3 + 5\ H_3PO_4 + 610\ H_2O \qquad (1)$$

This reaction proceeds until virtually all the O_2 has been consumed (Fig. 1, point B). At this point, if there were no diffusion, NO_3^- would rise to 51 μM, PO_4^{3-} to 3.26 μM, and ΣCO_2 to 2380 μM.

After oxygen has been depleted, oxidation by NO_3^- commences according to the general relation

$$5\ (CH_2O)_{106}\ (NH_3)_{16}(H_3PO_4) + 472\ HNO_3 \rightarrow 530\ CO_2 + 276\ N_2 + 886\ H_2O + 5\ H_3PO_4 \qquad (2)$$

A mole of NO_3^- oxidizes 46 percent more organic matter than does a mole of O_2, and by the completion of reaction 2 nitrate reduction is responsible for 25 percent of the metabolites produced. Reaction 2 proceeds until all 51 μM of NO_3^- are consumed, producing 57 μM of CO_2 and 0.54 μM of PO_4^{3-}. By point C (Fig. 1), 250 μM of O_2 and a net of 22 μM of NO_3^- have been consumed, whereas 249 μM of CO_2 and 2.35 μM of PO_4^{3-} have been produced.

Following NO_3^- exhaustion, oxidation continues by SO_4^{2-} reduction, according to the general relation

$$(CH_2O)_{106}(NH_3)_{16}(H_3PO_4) + 53\ SO_4^{2-} \rightarrow 106\ HCO_3^- + 16\ NH_3 + H_3PO_4 + 53\ H_2S \qquad (3)$$

In sediments where SO_4^{2-} reduction is significant, this process is responsible for most of the oxidation of organic matter, because the SO_4^{2-} available can oxidize 56,000 μM of CH_2O—roughly 225 times as much as oxygen and nitrate combined.

There are several ways in which a real system may deviate from the ideal reactions 1, 2, and 3 (*5*). First, NO_3^- may be removed in ways other than by oxidizing organic matter (reaction 2). For example, it is possible that nitrate-reducing bacteria will only oxidize either ammonia produced in the sulfate reduction zone or organic nitrogen according to the following idealized reaction (in which NH_3 can represent either ammonia or organic nitrogen)

$$3\ HNO_3 + 5\ NH_3 \rightarrow 4\ N_2 + 9\ H_2O \qquad (4)$$

Although there is no known bacterial species which mediates this reaction, we cannot rule out the possibility that such a species exists. Note that reaction 4 produces 2.28 times as much N_2 per mole of NO_3^- consumed as reaction 2. Second, NH_3 produced in the sulfate reduction zone may diffuse upward into the oxidizing zone and react with O_2 to produce nitrate. The nitrate maxima observed by Vanderborght and Billen (*6*) may be due to this effect. On the other hand, some ammonia produced as an intermediate in reaction 1 may not be oxidized to nitrate, resulting in the production of less nitrate than predicted. Third, intermediate steps in reaction 2 may produce NO_2^-, NO, N_2O, and so on, which may not be further reduced. Fourth, organic nitrogen liberated in reaction 2 may be released as ammonia rather than N_2. Fifth, the C/P and C/N ratios of organic matter in pelagic sediments may, as a result of selective fractionation during oxidation, differ from the Redfield ratios. In this case the reaction stoichiometry will differ from that in reactions 1 to 3, but the sense of the covariations will remain the same. In particular, the nitrate concentration, $[NO_3^-]$, will increase during O_2 reduction and decrease to zero during NO_3^- reduction. Thus, although our arguments assume that the thermodynamically stable products are produced in each case, and that the C/N and C/P ratios of the organic matter are equal to the Redfield ratios, we acknowledge that the situation in the real world may be more complex (*4*, *7*).

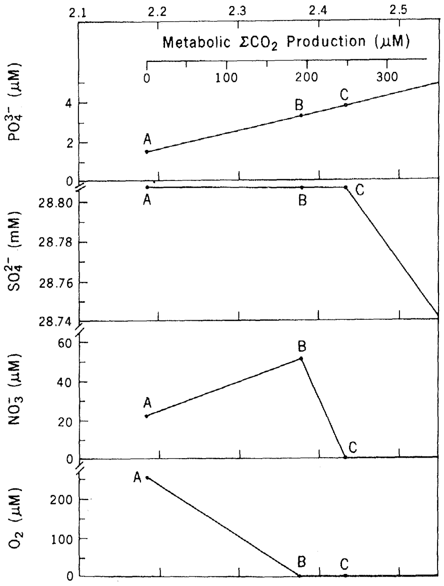

Fig. 1. Concentrations of metabolites (PO_4^{3-}, NO_3^-) and oxidants (O_2, SO_4^{2-}, NO_3^-) in a closed system as a function of metabolic CO_2 production. The curves were calculated from assumptions in the text. (Point A) North Atlantic deep water; (point B) composition at end of O_2 consumption; and (point C) composition at end of NO_3^- consumption.

The preceding discussion emphasizes the role of NO_3^- in the diagenesis of organic matter. Measurements of NO_3^- in pore waters of marine sediments provide information on the oxidation of organic matter above the SO_4^{2-} reduction zone and yield qualitative estimates of O_2 concentrations in pore waters. Of course, estimating $[O_2]$ from $[NO_3^-]$ in real pore-water systems is more complicated than in our simple model because of differences in O_2 and NO_3^- diffusion coefficients and uncertainties in the C/N ratio of oxidized organic matter. Nitrate data also identify the onset of SO_4^{2-} reduction, which can begin only below the depth at which nitrate is exhausted. Finally, pore-water nitrate data can contribute to a better understanding of fixed-nitrogen regeneration from various sediment types, and of rates of denitrification during nitrate reduction.

Results. We have determined NO_3^- plus NO_2^- in pore waters from sediments underlying relatively productive shelf, slope, and equatorial waters in the Guinea Basin (Fig. 2). All cores (except piston cores, discussed later) were obtained with a Benthos gravity corer, which was used without the core cutter, catcher, or barrel to prevent distortion of the sediment surface. Cores were extruded at in situ temperatures under a helium atmosphere. Pore waters were expressed at in situ temperatures with modified Reeburgh squeezers (*8*). The NO_3^- plus NO_2^- concentrations were determined in undiluted 1-ml samples by an AutoAnalyzer (Technicon method 158-71W), 1 hour to 1 day after squeezing. Details of procedures and concentrations of other dissolved species will be reported elsewhere (*9*).

Table 2. Comparison of nitrate and ammonia gradients in adjacent gravity cores and piston cores. The nitrate gradient is for the zone of linear decrease of concentration with depth.

Core	Location	Water depth (m)	$\delta[NO_3^-]/\delta z$ (10^{-3} μmole cm^{-4})	$\delta[NH_4^+]/\delta z$ (10^{-3} μmole cm^{-4})	$\frac{\delta[NH_4^+]/\delta z}{\delta[NO_3^-]/\delta z}$
24SC1	2°50.9′N, 6°41.0′W	4572	−0.93		−0.25
8PC1	2°55.1′N, 6°41.4′W	4535		0.23	
12GC2	0°04.1′N, 10°33.8′W	3880	−0.43		−0.37
20PC1	0°02.4′N, 10°35.9′W	3870		0.16	
11TW1	0°01.8′N, 9°03.9′W	4980	−0.97		−0.34
21PC1	0°02.4′N, 9°06.7′W	5029		0.33	

The NO_3^- profiles shown in Fig. 3 can be divided into two types. The first type includes cores 7, 27, and 28, which display nitrate concentrations of less than 3 μM throughout. These cores are from hemipelagic muds on the Ivory Coast shelf. Surface biological productivity is high and a permanent boundary layer of nutrient-rich, oxygen-poor water covers the shelf below a depth of about 30 to 40 m (*10*). Both oxygen and nitrate must be consumed in the upper centimeter, as sulfate reduction begins at this depth. Such a thin oxidizing layer is typical of nearshore, organic-rich sediments overlain by oxygen-depleted waters (*11*).

The second type of profile (cores 10, 11, 12, 14, and 16 in Fig. 3) resembles that generated by our simple model (Fig. 1) with the ΣCO_2 axis replaced by the depth axis. However, the subbottom NO_3^- maximum is 35 to 40 μM, rather than the predicted value of 51 μM. In part, this difference reflects both upward and downward diffusion of NO_3^- in the sediment column. The difference may also reflect a high C/N ratio in the oxidized organic matter, incomplete ammonia oxidation in the O_2 reduction zone, or one of several other possible deviations from our ideal model.

The NO_3^- profile for core 14 provides an example of the use, suggested earlier, of NO_3^- as an indicator of the diagenetic status of sediments. This core consisted of tan carbonate ooze (85 percent $CaCO_3$) down to a depth of about 40 cm, with dark gray, carbonate-poor terrigenous sediment below 40 cm. We can write the following equation (*12*) for the rate of change of the NO_3^- concentration of pore water at a depth z below the sediment-water interface

$$\frac{d\phi[NO_3^-]}{dt} = I(NO_3^-)\, d\left(\phi D_a \frac{d[NO_3^-]}{dz}\right) - \frac{d(\phi W[NO_3^-])}{dz} + I(NO_3^-)\delta J \qquad (5)$$

where t is time, z is depth relative to the sediment-water interface, ϕ is porosity, $I(NO_3^-)$ is a term to account for adsorption of nitrate onto sediment, D_a is the apparent diffusion coefficient (*13*) of nitrate, W is the upward flux of water due to compaction, and J is the production rate ($J > 0$) or consumption rate ($J < 0$) of nitrate. We assume that there is no absorption of NO_3^- [hence $I(NO_3^-) = 1$]; that the pore-water nitrate profile is a steady state feature ($d[NO_3^-]/dt) = 0$, and that the advective flux term $d(\phi W[NO_3^-])/dz$ is negligible; and we note that in the critical depth range of 2 to 31 cm the porosity (and hence the diffusion coefficient) is constant (the mean and total range of nine porosity measurements in this depth range is 0.74 ± 0.02 by volume). With these assumptions and observations, Eq. 5 simplifies to

$$J = -D_a \frac{d^2[NO_3^-]}{dz^2} \qquad (6)$$

Near the top of the core, where $d^2[NO_3^-]/dz^2 < 0$ (0 to 5 cm), $J > 0$ and nitrate is being produced; oxygen is presumably present. Where $d^2[NO_3^-]/dz^2 = 0$ and $[NO_3^-] > 0$ (5 to 34 cm), $J = 0$ and we infer that no detectable oxidation of organic matter is occurring. Where $d^2[NO_3^-]/dz^2 > 0$ (somewhere between 34 and 41 cm), $J < 0$ and nitrate reduction is occurring. The oxidation zone at 0 to 5 cm presumably reflects the presence of O_2 and labile organic matter in the young sediments; the relatively rapid rate of nitrate reduction at 34 to 41 cm probably reflects an increase in the reactive organic carbon content below the 40-cm lithologic break. Finally, where $[NO_3^-] = 0$ (depths > 41 cm), diagenesis of organic matter is occurring (if at all) by SO_4^{2-} reduction.

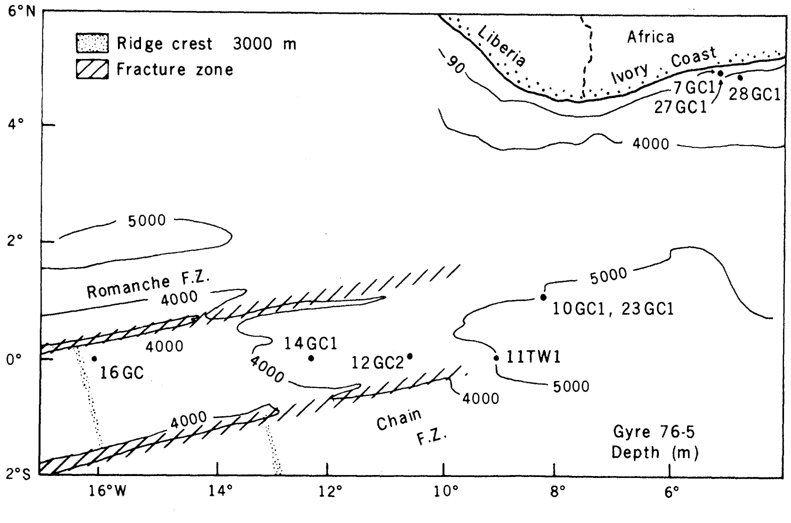

Fig. 2. Map showing core locations. Depth contours are in meters.

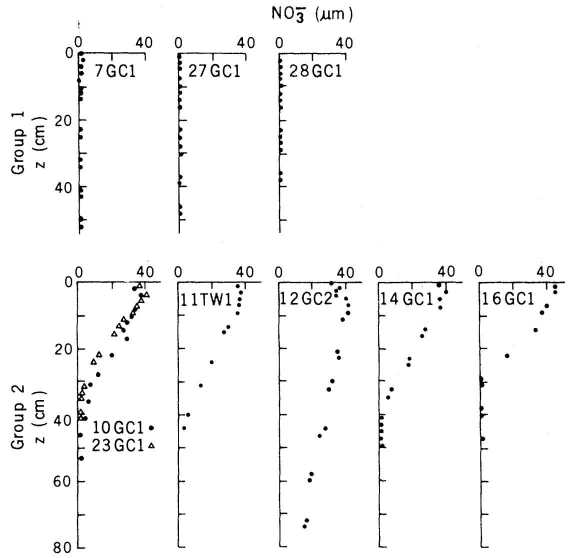

Fig. 3. Nitrate concentration as a function of depth in eastern equatorial Atlantic gravity cores. Where the cores in group 2 were raised, the bottom water nitrate concentration is about 22 μM.

In the introductory discussion, we suggested that significant NO_3^- could be consumed in oxidizing ammonia. We can check this possibility by comparing the downward flux of NO_3^- in our gravity cores with the upward flux of NH_3 in nearby piston cores, and calculating whether ammonia is diffusing to the NO_3^- reduction zone sufficiently rapidly to consume all the NO_3^-. Ammonia increases linearly with depth in the piston cores, so there is little uncertainty in the gradient or flux estimates.

Estimated NO_3^- and NH_4^+ gradients are compared in Table 2. According to reaction 4, if diffusion alone transports NO_3^- and NH_3 to the reaction sites, and if all NO_3^- is consumed by NH_3 oxidation, then it must hold that

$$\frac{NH_4^+ \text{ flux}}{NO_3^- \text{ flux}} \leq \frac{-5}{3}$$

Since flux = $D_a\, dC/dz$, then

$$\frac{(dC/dz)_{NH_4^+}}{(dC/dz)_{NO_3^-}} \leq \frac{-5}{3}\,\frac{D_a(\text{nitrate})}{D_a(\text{ammonia})}$$

where dC/dz is the observed interstitial gradient and D_a is the apparent interstitial diffusion coefficient. Since the aqueous diffusion coefficients of nitrate and ammonia at infinite dilution are nearly equal (*13*), we assume that the ratio of D_a(nitrate) to D_a(ammonia) is one. From Table 2, it is clear that the observed NH_3 flux below the nitrate reduction zone is insufficient to consume more than 15 to 25 percent of the NO_3^- sink. Our NH_3 data for the O_2 reduction and NO_3^- reduction zones are too uncertain to reveal NH_3 behavior in these portions of the sediment column.

We may estimate both the benthic flux of NO_3^- and the consumption rates of fixed nitrogen (denitrification) at the pelagic sediment sites (cores 10 to 16) from the data of Fig. 3 and Table 2. The average NO_3^- gradient at the sediment-water interface is taken as 20×10^{-3} μM cm^{-4} (this gradient is calculated assuming that the $[NO_3^-]$ in the top centimeter of the sediment is 32 μM, compared with 22 μM in the bottom water, and that the gradient increases linearly in the top centimeter: it is the minimum gradient necessary to account for the observation that the nitrate concentration of the top centimeter of the sediment is approximately 10 μM higher than the bottom water value). Note that, if we consistently lost material at the sediment-water interface during coring, the real gradient must be less than our assumed value. The gradient in the zone of linear decrease of nitrate with depth is taken as -0.9×10^{-3} μM cm^{-4}.

Apparent diffusion coefficients of NO_3^- and NH_4^+ were estimated by multiplying the value at 0°C and infinite dilution (*13*) by the product of the tortuosity factor of 0.55 (*14*) and a porosity of 0.75 (porosities measured in duplicates of cores 12 and 16 averaged 0.76 ± 0.05 and 0.74 ± 0.02, respectively). This gives a value of D_a for both NO_3^- and NH_4^+ of 4.0×10^{-6} cm^2 sec^{-1}.

From these diffusion coefficients and the concentration gradients given above, we estimate that the benthic flux of NO_3^- across the sediment-water interface is about 2.5 μM cm^{-2} $year^{-1}$. This flux integrates the total nitrate production between the sediment-water interface and the depth of the nitrate maximum. The downward flux of NO_3^- in the zone of linear decrease is about 0.11 μM cm^{-2} $year^{-1}$; this flux integrates the nitrate production below the depth of the nitrate maximum. Thus, of the NO_3^- produced by oxidative regeneration in these cores, about 96 percent is returned to the overlying ocean and 4 percent is consumed by denitrification.

These calculated fluxes can be compared to the global rate of input of NO_3^- to the deep ocean, which can be estimated from the nitrate content of a 1-cm^2 column of North Pacific deep water. Assuming an "age" of 1600 years (*15*), an average depth of 3500 m (and therefore a volume of 350 liter cm^{-2}), and an NO_3^- concentration of 40 μM, the rate of input of nitrate is

$$\frac{(40\ \mu M\ \text{liter}^{-1})(350\ \text{liter cm}^{-2})}{1600\ \text{years}} = 8.8\ \mu M\ \text{cm}^{-2}\ \text{year}^{-1}$$

This is more than three times the benthic flux of nitrate at our eastern equatorial Atlantic stations. Inasmuch as our stations underlie a productive upwelling area, the benthic flux we have calculated is likely to be much higher than the global average value. These results are consistent with the view that most phosphorus and fixed nitrogen input to deep waters occurs in the upper part of the deep-water column rather than at the deep-sea floor (*16*).

According to reaction 2, 1.17 moles of N are freed for every mole of NO_3^- reduced. If this reaction accurately describes the mode and stoichiometry of NO_3^- consumption, the rate of denitrification is 1.17 times the downward NO_3^- flux, or about 0.13 μM of N per square centimeter per year. Alternately, if reaction 4 is responsible for NO_3^- reduction, then 2.67 moles of N are freed for every mole of NO_3^- reduced, and the calculated denitrification rate is 0.29 μM of N per square centimeter per year.

On the basis of published estimates of marine denitrification and considerations of the global nitrogen balance, it has been concluded (*17*) that oceanic denitrification is of the order of 10 to 70 megatons of N per year. If NO_3^- reduction is occurring in all marine pelagic sediments at the same rate as in our Guinea Basin cores (and assuming the stoichiometry is as indicated in reaction 2), it could account for a total denitrification of about 5 megatons of N per year. In the eastern tropical North Pacific, the most important site of marine denitrification yet identified, denitrification is occurring at the rate of about 20 megatons of N per year (*18*). While denitrification is undoubtedly occurring less rapidly over the deep ocean as a whole than at our study site underlying a tropical upwelling area, our results suggest that pelagic sediments cannot be dismissed as possible significant sites of marine denitrification. In other words, while pelagic denitrification has not been proved to be a major global sink of fixed nitrogen, it cannot be neglected in light of existing uncertainties in the nitrogen balance.

MICHAEL L. BENDER
Graduate School of Oceanography,
University of Rhode Island,
Kingston 02881
KENT A. FANNING
Department of Marine Sciences,
University of South Florida,
St. Petersburg 33701
PHILIP N. FROELICH
G. ROSS HEATH
Graduate School of Oceanography,
University of Rhode Island
VALENTINE MAYNARD
Department of Marine Sciences,
University of South Florida

References and Notes

1. R. A. Berner, in *The Sea* (Wiley-Interscience, New York, 1974), vol. 5, pp. 427–450; V. Grundmanis, and J. W. Murray, *Limnol. Oceanogr.*, in press.
2. A. C. Redfield, *Am. Sci.* **4**, 205 (1958).
3. ———, B. H. Ketchum, F. A. Richards, in *The Sea* (Wiley-Interscience, New York, 1963), vol. 2, pp. 20–77.
4. F. A. Richards, in *Chemical Oceanography* (Academic Press, New York, 1965), vol. 1, pp. 611–645.
5. R. O. Barnes, K. K. Bertine, E. D. Goldberg, *Limnol. Oceanogr.* **20**, 962 (1975).
6. J.-P. Vanderborght and G. Billen, *ibid.*, p. 953.
7. W. Stumm and J. J. Morgan, *Aquatic Chemistry* (Wiley-Interscience, New York, 1970), pp. 300–377.
8. W. S. Reeburgh, *Limnol. Oceanogr.* **12**, 163 (1967).
9. P. N. Froelich, B. Hammond, D. Hartmann, G. R. Heath, M. Bender, in preparation.
10. D. W. McGrail, thesis, University of Rhode Island (1976).
11. E. Sholkovitz, *Geochim. Cosmochim. Acta* **37**, 2043 (1973).
12. R. A. Berner, *Am. J. Sci.* **275**, 88 (1975).
13. Y. H. Li and S. Gregory, *Geochim. Cosmochim. Acta* **38**, 703 (1974).
14. M. L. Bender, *J. Geophys. Res.* **76**, 4212 (1971).
15. W. Broecker, *Chemical Oceanography* (Harcourt Brace Jovanovich, New York, 1974).
16. J. M. Edmond, *Deep Sea Res.* **21**, 455 (1974).

17. Council for Agricultural Science and Technology, *Effect of Increased Nitrogen Fixation on Stratospheric Ozone* (Report 53, Department of Agronomy, Iowa State University, Ames, 1976).
18. L. A. Codispoti and F. A. Richards, *Limnol. Oceanogr.* **21**, 379 (1976).

19. We gratefully acknowledge D. Hammond, B. Hartmann, G. P. Klinkhammer, N. Luedtke, D. Cullen, and the crew of R./V. *Gyre*, cruise 76-05, for support in carrying out the shipboard measurements. We are indebted to M. Pilson for criticism and discussions. This research was supported by NSF grant OCE-76-02318 to M.L.B. and G.R.H. and by NSF grants GA 41200 and OCE 76-82416 to K.A.F.

23 March 1977; revised 27 June 1977

Ocean Wave Patterns Under Hurricane Gloria: Observation with an Airborne Synthetic-Aperture Radar

Abstract. *Surface imagery of ocean waves under Hurricane Gloria (September 1976) has been obtained with an airborne synthetic-aperture imaging radar. Observations were obtained over most of the area within a radius of 150 kilometers around the center of the eye. These direct observations made it possible to derive the wave patterns in the region around a hurricane eye.*

Observations of ocean wave patterns near a hurricane center are practically nonexistent. High-altitude aircraft observations with cameras are not generally possible because of extensive cloud cover. Flights at very low altitude with laser profilometer observations have been conducted on some occasions (*1, 2*); however, they are limited to a very small coverage along the aircraft track and contain no directional information. Direct surface measurements by ships near the eye are few because of the sea conditions, and they are limited in coverage. Pore (*3*) has collected a large number of visual ship reports in a variety of hurricanes and studied the spatial distribution of wave properties. However, most of the reported observations were at a distance greater than 130 km from the hurricane's center. There also have been a few surface point measurements of hurricane waves from offshore platforms (*4*) and from instrumented buoys (*5*).

Recently, high-resolution imagery of ocean waves and surface patterns obtained with airborne radar systems has been reported (*1, 6*). The direction and wavelength of the ocean waves can be directly determined from the radar image. However, the relationship between the radar signature and the wave characteristics, such as the directional energy spectrum, is not well understood and is an area of active research. One major advantage of the imaging radar is that, with the proper selection of frequency, it is insensitive to cloud cover. Another is that it does not require sun illumination. A further key factor is that, if operated in a coherent synthetic-aperture mode, it can obtain high-resolution imagery from high-altitude airborne or spaceborne platforms.

These considerations led us to conduct an experiment to observe the ocean surface under hurricanes Emmy, Frances, and Gloria in the summer of 1976. The aircraft used was the National Aeronautics and Space Administration Ames CV-990 jet, which flew over these hurricanes at altitudes ranging from 8,000 to 13,000 m. The aircraft was equipped with the Jet Propulsion Laboratory synthetic-aperture, multifrequency-imaging radar, which was operated at 1.2 and 9.6 Ghz. The inherent resolution of the system is between 25 and 50 m, depending on the "look" angle. Thus, only waves of wavelengths equal to or larger than about 75 m can be clearly imaged with this sensor. Continuous imagery, with a 10-km swath, was obtained on two perpendicular legs centered at the eye and extending radially to approximately 150 km to each side of the eye. Imagery was also obtained along two octagonal flight lines centered at the eye with average radii of about 50 and 140 km.

The data discussed in this report were obtained on 30 September 1976, during Hurricane Gloria. At the start of the observations (at 1600 G.M.T.), the hurricane center was located 650 km northeast of Bermuda at 58°00′W, 32°40′N and was moving with a speed of 28 km/hour in a northeasterly direction. The maximum surface wind, reported by a low-flying National Oceanic and Atmospheric Administration (NOAA) aircraft, was 60 m/sec, and the radius to maximum wind was approximately 60 km. The observation period lasted about 4 hours.

The wind field was counterclockwise with a slight inward spiral, as is typical for hurricanes in the Northern Hemisphere. The wind field was stronger on the right side of the storm, as seen facing the direction of storm movement. This is also typical; for, if a hurricane is to remain an organized unit, the winds must blow faster in the direction of storm travel than against it. This leads to a substantial asymmetry in the wave field under a

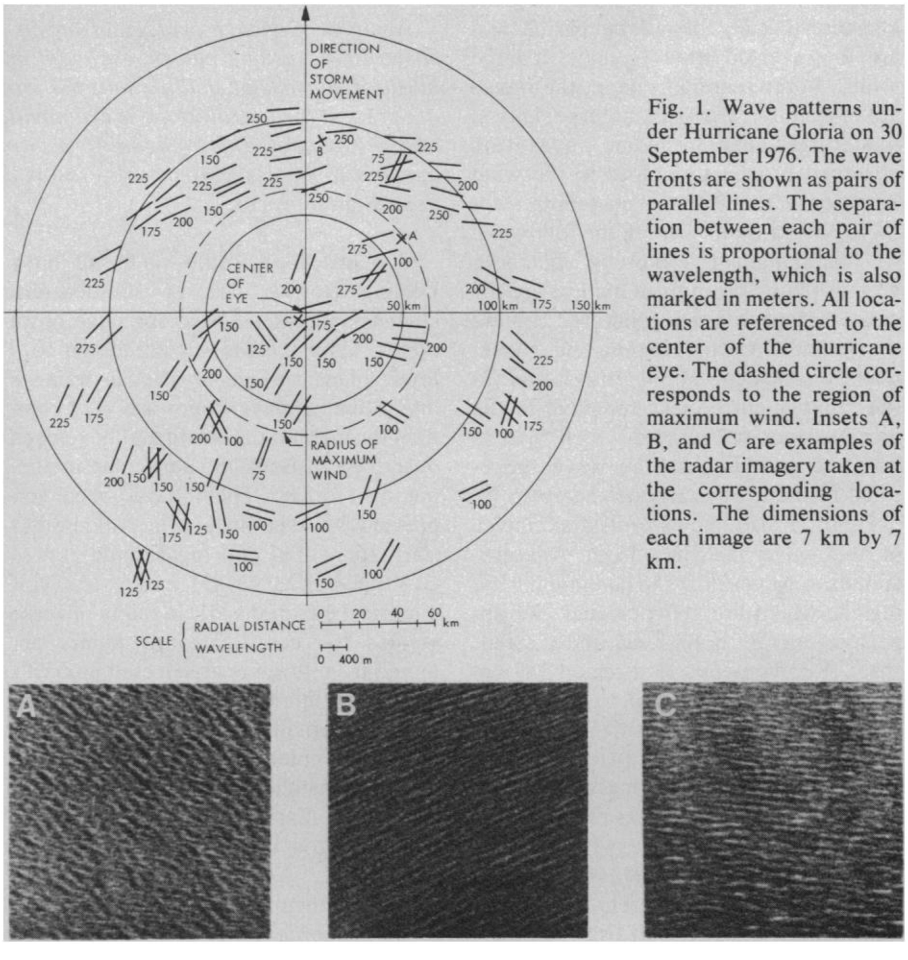

Fig. 1. Wave patterns under Hurricane Gloria on 30 September 1976. The wave fronts are shown as pairs of parallel lines. The separation between each pair of lines is proportional to the wavelength, which is also marked in meters. All locations are referenced to the center of the hurricane eye. The dashed circle corresponds to the region of maximum wind. Insets A, B, and C are examples of the radar imagery taken at the corresponding locations. The dimensions of each image are 7 km by 7 km.